Identifying single-cell molecular programs by stochastic profiling

Kevin A Janes[1,2], Chun-Chao Wang[2], Karin J Holmberg[2], Kristin Cabral[3] & Joan S Brugge[1]

Cells in tissues can be morphologically indistinguishable yet show molecular expression patterns that are remarkably heterogeneous. Here we describe an approach to comprehensively identify co-regulated, heterogeneously expressed genes among cells that otherwise appear identical. The technique, called stochastic profiling, involves repeated, random selection of very small cell populations via laser-capture microdissection followed by a customized single-cell amplification procedure and transcriptional profiling. Fluctuations in the resulting gene-expression measurements are then analyzed statistically to identify transcripts that are heterogeneously coexpressed. We stochastically profiled matrix-attached human epithelial cells in a three-dimensional culture model of mammary-acinar morphogenesis. Of 4,557 transcripts, we identified 547 genes with strong cell-to-cell expression differences. Clustering of this heterogeneous subset revealed several molecular 'programs' implicated in protein biosynthesis, oxidative-stress responses and NF-κB signaling, which we independently confirmed by RNA fluorescence *in situ* hybridization. Thus, stochastic profiling can reveal single-cell heterogeneities without the need to measure expression in individual cells.

Cell-to-cell variations in gene and protein expression are important in the development and function of many tissues[1,2]. Fluctuations in single cells can be masked or completely misrepresented when populations are analyzed[3]. This makes heterogeneities problematic for interpreting bulk measurements from large numbers of cells, such as from tumors or developing organs. Yet such nonuniformities often uncover interesting molecular patterns that can reveal important mechanisms for the regulation of cell fate[4,5]. Identifying heterogeneities is thus key for gaining a deeper understanding of tissue physiology.

The challenge in discovering heterogeneities is that cells of the same type may appear phenotypically indistinguishable. Heterogeneities at the molecular level can be uncovered by immunochemistry, but the markers must be selected a priori and analyzed in small groups. Although more parameters can be screened simultaneously with flow cytometry[3], this involves substantial tissue processing to isolate single cells from solid tissues. Extraction of individual cells is possible *in situ* using laser-capture microdissection[6], but aside from large cells such as neurons and cardiomyocytes[7,8], there is usually not enough biological material to measure the expression of all but the most abundant transcripts.

Last and most importantly, there is the conceptual hurdle of interpreting measurements from a single cell. Regulated cell-to-cell heterogeneities will appear as fluctuations in one-cell measurements. However, fluctuations will also be observed because of random biological variation, which may be functionally inconsequential[9], and measurement error, which can be enormous[10]. The inability to separate contributions from these different sources has precluded using single-cell approaches to study the coordination of pathways that are heterogeneously activated.

We sought to address these challenges by developing an approach, called stochastic profiling, which is based on small-population averaging of randomly chosen cells. Using this approach, we examined single-cell gene expression in a three-dimensional (3D) culture model of mammary-acinar morphogenesis[11]. The sensitivity, precision and quantitative accuracy of stochastic profiling make it an attractive technique for studying endogenous transcriptional heterogeneities in development and cancer.

RESULTS

Stochastic sampling of expression dichotomies

To reveal the dichotomous expression of a gene (gene *B*), which has high expression in one population and low expression in another (**Fig. 1a**), we first repeatedly selected very small cell populations at random and measured the average gene expression in each random sampling. Second, we constructed a reference histogram from expression data for homogeneously expressed genes (gene *A*), which estimate the sampling fluctuations when no dichotomy is present. Last, we compared the estimated reference distribution to the distribution of expression fluctuations for candidate genes measured from the same stochastic samplings (step 3). The gene *B* distribution will deviate from the gene *A* reference because of differences in the proportion of subpopulations collected at each sampling (**Fig. 1a**). Additionally, dichotomously expressed genes that are co-regulated at the single-cell level (gene *B* and the

[1]Department of Cell Biology, Harvard Medical School, Boston, Massachusetts, USA. [2]Department of Biomedical Engineering, University of Virginia, Charlottesville, Virginia, USA. [3]Molecular Genetics Core Facility, Children's Hospital Boston and Harvard Medical School, Boston, Massachusetts, USA. Correspondence should be addressed to K.A.J. (kjanes@virginia.edu) or J.S.B. (joan_brugge@hms.harvard.edu).

RECEIVED 26 OCTOBER 2009; ACCEPTED 22 FEBRUARY 2010; PUBLISHED ONLINE 14 MARCH 2010; DOI:10.1038/NMETH.1442

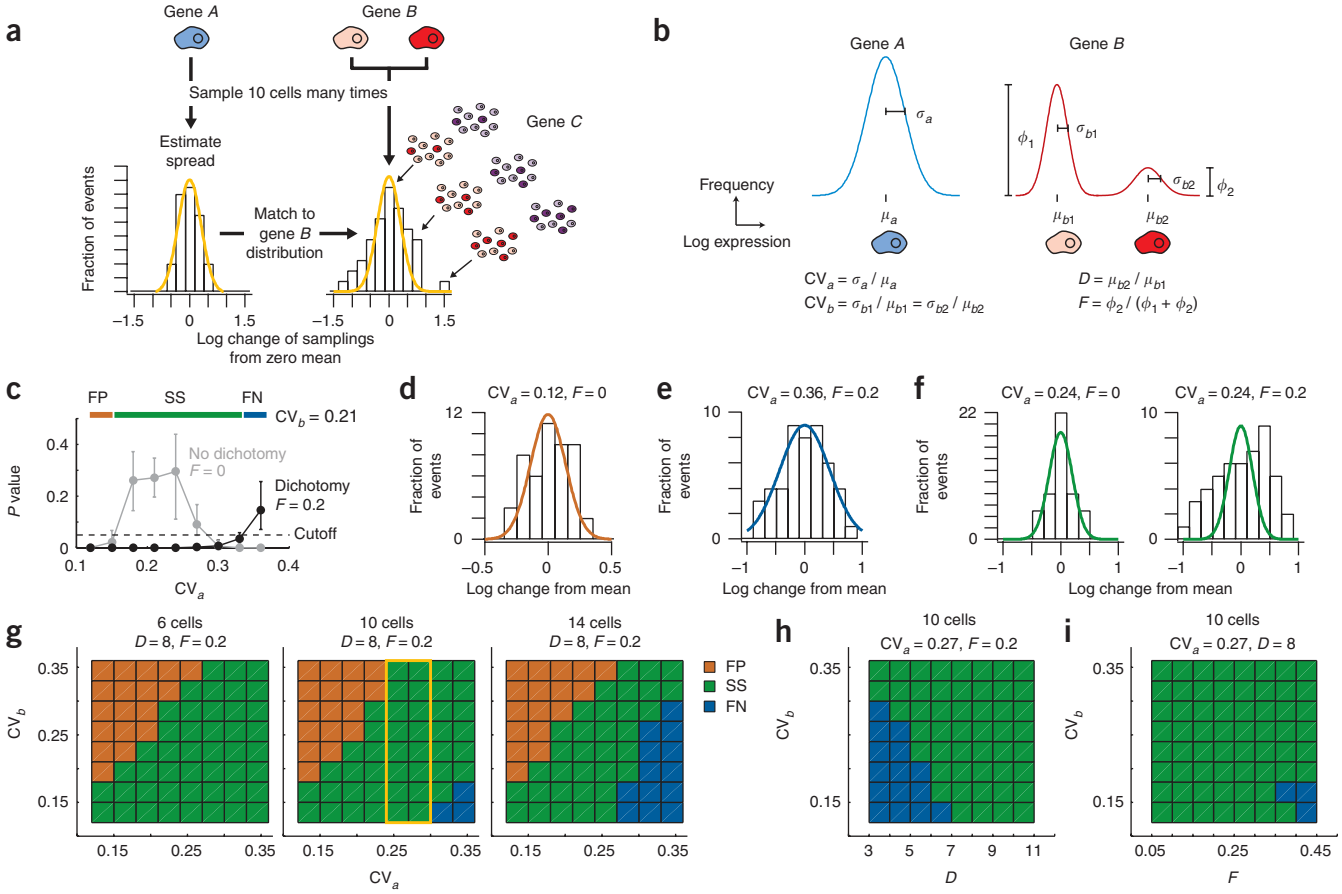

Figure 1 | Small-sample profiling by stochastic sampling can be used to distinguish transcriptional heterogeneities from normal biological variation. (**a**) The statistical and empirical steps of stochastic sampling. The distributions shown were based on 48 simulated samplings with the following model parameters: CV_a = 25%, CV_b = 25%, D = 8 and F = 0.2. (**b**) Theoretical population distributions of a constitutively expressed gene (gene *A*) and a dichotomy with two subpopulations (gene *B*). Gene *A* is characterized by its mean (μ_a) and s.d. (σ_a), and gene *B* is characterized by the means (μ_{b1} and μ_{b2}) and s.d. (σ_{b1} and σ_{b2}) of the two subpopulations along with the relative fractions of each subpopulation (ϕ_1, ϕ_2). (**c**) Identifying false positives (FP), false negatives (FN) and effective stochastic sampling (SS) through Monte Carlo simulations. Stochastic-sampling experiments were simulated as described in Online Methods with the indicated parameters and D = 8. Data are shown as the median P value for the χ^2 goodness of fit between the test and reference distributions ± 90% nonparametric confidence intervals (error bars) from n = 50 simulations of 48 samplings. (**d**–**f**) Examples of false positives (**d**), false negatives (**e**) and effective stochastic sampling (**f**) for D = 8 and CV_b = 0.21. (**g**) Stochastic sampling with indicated numbers of averaged cells. Note that when 10 cells are averaged and CV_a = 25–30% (yellow box), stochastic sampling is effective for all values of CV_b. (**h**) Stochastic sampling for dichotomies with expression differences greater than fivefold. (**i**) Stochastic sampling is not strongly dependent on the relative proportion of subpopulations in a dichotomy.

co-regulated dichotomy, gene *C*) will have deviations that correlate across repeated samplings. Therefore, we can, in principle, identify heterogeneous expression programs composed of multiple genes by clustering patterns of sampling fluctuations.

Theoretical validation of stochastic sampling

We used computer simulations to help define the required sampling conditions and characterize the expression heterogeneities that stochastic sampling detects. Cells transcribe genes in exponential 'bursts'[12], which yields log-normal probability distributions of mRNA species when examined across a cell population[13] (see below). We modeled gene expression in single cells as normal probability distributions with coefficients of variation (CVs) proportional to log-s.d. (**Fig. 1b**). The overall model described the reference and dichotomous distributions with four parameters: the CV of the reference distribution (CV_a), the CV of the distributions in the gene that is dichotomously expressed (CV_b), the magnitude of the expression difference between the dichotomous subpopulations (D) and the fraction of cells with high expression for the gene that is dichotomously expressed (F) (**Fig. 1b**).

After selecting values for CV_a, CV_b, D and F, we simulated the stochastic-sampling experiments and centered the expression fluctuations of each gene on its log-mean expression taken across all samplings (**Fig. 1a**). Next, we compared the sampling fluctuations of the dichotomously expressed gene to a log-normal distribution using the log-s.d. calculated from the reference distribution. We then assessed the discrepancy between the log-normal reference distribution and the sampling fluctuations of the dichotomously expressed gene for statistical significance by a χ^2 goodness-of-fit test (Online Methods).

As a control for the modeled stochastic samplings, we simulated a parallel set of control samplings, in which all the parameters were the same, but F was set to zero (that is, no dichotomy). These control samplings identified false positives, which were scored as different from the reference simply because the model CVs were poorly matched ($CV_a << CV_b$; **Fig. 1c**,**d**). When the reference and

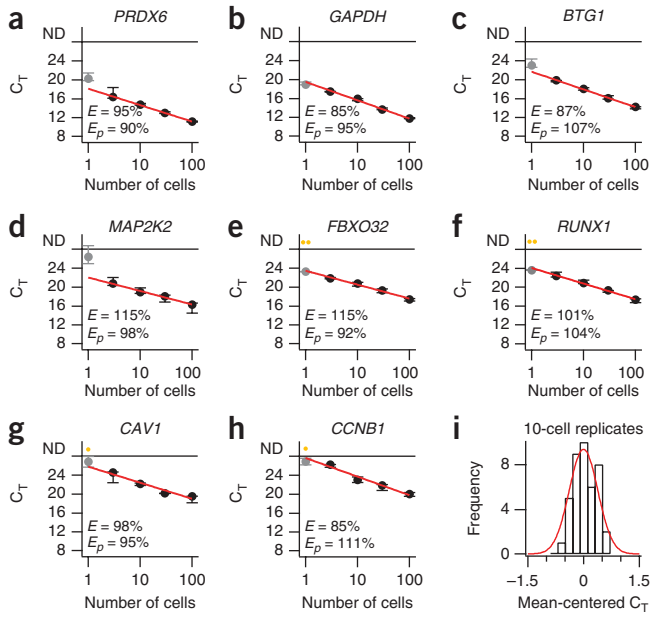

Figure 2 | Quantitative and reproducible small-sample amplification of high-, medium- and low-abundance transcripts from 3–100 cells. (**a**–**h**) The real-time qPCR cycle threshold (C_T) for each gene plotted as a function of starting cellular material and is shown as the median with error bars indicating the range of three replicate small-sample amplifications. Amplification efficiencies (E) based on a log-linear fit of the 3–100-cell dilutions (red line) are listed along with primer efficiencies (E_p) calculated by serially diluting the template before real-time qPCR analysis. Results (**a**–**h**) are given in the order of increasing median cycle threshold from the 10-cell replicates, which was used as an approximation of relative abundance (lower cycle thresholds suggest increased relative abundance). Note that the one-cell amplifications (gray data point) of higher-abundance transcripts (**a**–**d**) often deviate from the log-linear fit, and the one-cell amplification of lower-abundance transcripts (**e**-**h**) are frequently not detectable (ND; yellow). (**i**) Small-sample amplification of 10 cells. The cycle thresholds from 10-cell amplification replicates of all genes were mean centered, grouped and fit to a normal distribution. The s.d. of the mean-centered cycle thresholds was 0.36, corresponding to a coefficient of variation of 28%, assuming that amplicons doubled after each cycle (that is, 100% efficiency, $2^{0.36} - 1 = 0.28$).

dichotomy CVs were poorly matched in the opposite direction, $CV_a >> CV_b$, there was the danger of false negatives because a dichotomous sampling distribution could be misinterpreted as a log-normal distribution with a larger CV (**Fig. 1c**,**e**). Effective stochastic sampling occurred when the reference and dichotomy CVs were roughly comparable, so that significant deviations from the reference were observed only when $F \neq 0$ ($P < 0.05$; **Fig. 1c**,**f**).

We first determined the maximum number of cells that, when expression data were averaged, could be used to confidently identify heterogeneities across a wide range of CV_b. Direct estimates of transcriptional noise are not available, but studies in yeast have found that protein levels can fluctuate with CVs of ~12–38% (ref. 14). We independently varied CV_a and CV_b over this range for different numbers of cells sampled and then identified the CV combinations that gave false positives, false negatives and effective stochastic sampling. When CV_a was very low (<20%), we found that there was a substantial likelihood of false positives, which was independent of the number of cells sampled (**Fig. 1g**). Conversely, when CV_a was very high (>30%), there was a danger of false negatives, which increased dramatically when we sampled more than 10 cells (**Fig. 1g**). With 10-cell samplings and an intermediate reference distribution (CV_a of ~25–30%), we achieved effective stochastic sampling across nearly all CV_b values (**Fig. 1g**). Using these parameters, stochastic sampling could identify dichotomies as small as five- to sixfold (**Fig. 1h**), with relatively little dependence on the dichotomy fraction above ~5% (**Fig. 1i**). When $F < 0.05$, the dichotomy was too rare to detect reliably in 10-cell samplings, and we observed a sharp increase in the number of false negatives (**Supplementary Fig. 1**). We conclude that stochastic sampling of up to 10 cells is sufficient to detect many dichotomies when given a reference for the 'average' non-dichotomous sampling fluctuations.

Optimization of small-sample PCR for stochastic profiling

Based on the simulation-derived estimates, we then developed a poly(A)-PCR amplification procedure to profile gene expression accurately in 10 microdissected cells. Poly(A) PCR can be used to amplify large quantities of polyadenylated transcripts from minute samples[15]. This technique has previously been modified to improve either single-cell representation of genes or detection sensitivity for low-abundance transcripts[10,16]. To optimize the technique for stochastic sampling, we designed a 'small-sample' poly(A) PCR that maximizes both the reproducibility between measurement replicates and the quantitative accuracy of genes measured from 10 cells (**Supplementary Fig. 2** and Online Methods). We validated accuracy and precision by serially diluting microdissected cells before the amplification and then quantifying relative gene expression after amplification by real-time quantitative PCR (qPCR). The dilutions were critical to ensure that quantitative differences in transcript amounts were not artificially increased or decreased during the procedure. To date, this quantitative accuracy has only been shown when amplification is omitted entirely[17], which substantially limits the number of transcripts that can be analyzed from the same sample.

For 24 genes of differing abundance, we found that small-sample poly(A) PCR was highly accurate and reproducible for 3–100 cells (**Fig. 2a**–**h** and **Supplementary Fig. 3**). The median amplification efficiency (E) across all genes measured was 99.5%, and for individual genes, the efficiency of small-sample poly(A) PCR was comparable to the amplification efficiency of the real-time qPCR primers used for quantification (E_p). This suggested that the poly(A)-PCR procedure was not skewing changes in the abundance of individual genes. Overall, 10-cell reproducibility as measured by real-time qPCR was 0.36 cycle thresholds (C_T), which corresponds to an amplification precision of ~28% if $E = 100\%$ ($2^{0.36} - 1 = 28\%$; **Fig. 2i**). Notably, for many genes the accuracy and precision of poly(A) PCR decreased substantially when single-cell equivalents of RNA were used (**Fig. 2a**–**h** and **Supplementary Fig. 3**). Several genes were not reproducibly detectable (**Fig. 2e**–**h**), whereas others deviated from the log-linear standard predicted from the 3–100-cell dilution series (**Fig. 2a**,**c**,**d**). We obtained these results for microdissected breast epithelial cells with an average diameter of ~10 μm. Therefore, many more cell types should be quantifiable using a small-sample (rather than single-cell) approach together with stochastic profiling.

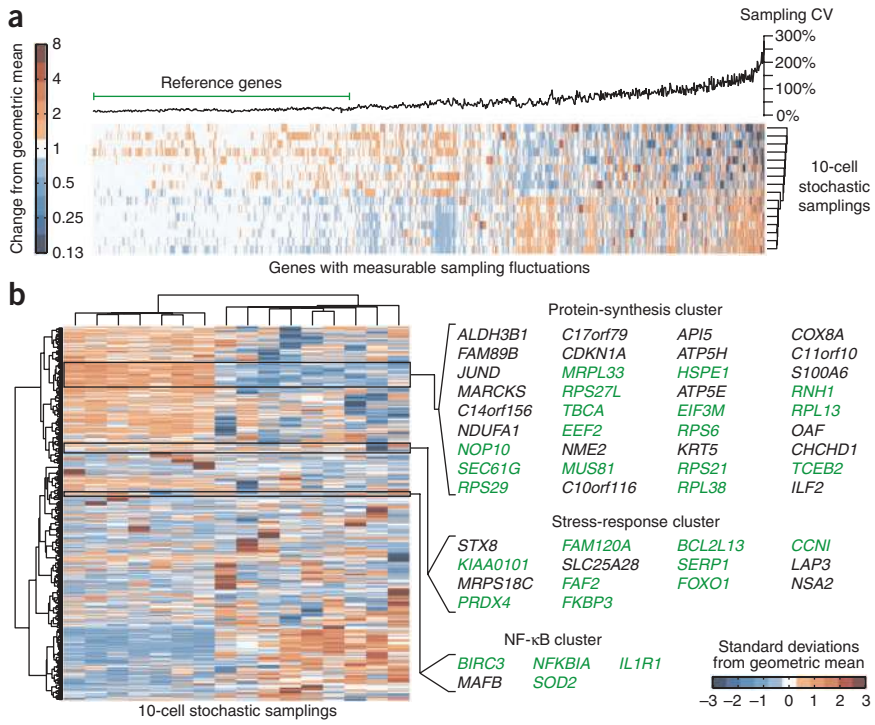

Figure 3 | Stochastic profiling of matrix-attached cells at day 10 of MCF10A morphogenesis. (**a**) Hierarchical clustering of unscaled sampling fluctuations for transcripts with measurable biological variation. Genes with sampling variations greater than measurement error were clutered using a Euclidean distance metric and average linkage. The genes with consistent CV values (left) were used as the reference subset for calculating an appropriate reference distribution to test for heterogeneous expression. (**b**) Hierarchical clustering of scaled sampling fluctuations for transcripts predicted to be heterogeneously expressed by stochastic profiling. Candidate heterogeneities were scaled to unit variance and clustered using a Euclidean distance metric and Ward's linkage. Selected clusters were examined for enriched biological functions. Genes consistent with the assigned functions are in green.

Adapting small-sample PCR to oligonucleotide microarrays

A key step in accurate 10-cell quantification was limiting the number of amplification cycles in small-sample poly(A) PCR to no more than 30 (**Supplementary Fig. 2**). With 10 microdissected cells, a 30-cycle amplification typically yielded ~10 ng of unlabeled cDNA, which was insufficient for oligonucleotide microarrays. We therefore reamplified a fraction of the poly(A) cDNA and added aminoallyl-dUTP for subsequent fluorophore labeling, yielding ~1.5 μg of labeled cDNA per 10-cell sample. The conditions for reamplification differed from small-sample poly(A) PCR (Online Methods), and we carefully monitored the conditions with real-time pilot experiments to identify the maximum number of cycles that kept all samples in the exponential phase of amplification. Doing so maintained the quantitative accuracy for high- and low-abundance transcripts (**Supplementary Fig. 4**). Furthermore, repeat reamplifications using the same starting cDNA pool confirmed that reamplification added little measurement error to the final microarray measurements (**Supplementary Fig. 5**). Hybridization of reamplified samples to Illumina HumanRef-8 microarrays consistently detected 7,000–8,000 transcripts (median detection $P < 0.1$). This result compares favorably with an earlier study from our group[18], in which ~8,700 transcripts had been detected by standard profiling approaches using RNA extracted from large populations of the cells used here. We conclude that our experimental platform is sufficiently accurate and sensitive to quantify much of the transcriptome for stochastic profiling.

Stochastic profiling of epithelial acinar morphogenesis

As a proof of principle, we tested the feasibility of stochastic profiling in a 3D culture model of mammary epithelial acinar morphogenesis[11]. We seeded individual MCF10A mammary epithelial cells in reconstituted basement membrane under conditions that promote the formation of proliferation-arrested, hollow acinar structures comprised of 50–100 cells when fully mature. Each acinus is clonal and thus isogenic, but many signaling and cell-fate dichotomies nonetheless emerge during morphogenesis. For example, matrix-attached cells of the outer acinus appear grossly similar but have variable expression of phospho-Akt[19], phospho-myosin light chain[20] and the CDK inhibitor p27 (ref. 21). The overall extent of such cell-to-cell heterogeneities and their role in morphogenesis has not been defined.

We focused the stochastic profiling on matrix-attached cells in developing 3D cultures because these cells comprise the final acinar structure that resembles the lobular unit of the breast *in vivo*[11]. Matrix-attached cells are also readily identified in cryosections of 3D structures and can be microdissected as single cells with high accuracy (**Supplementary Fig. 6** and Online Methods). We obtained transcriptional profiles for 16 independent 10-cell samplings of matrix-attached cells along with 16 measurement controls. The control samples consisted of independent amplifications from a common starting pool of 160 microdissected cells. These amplification replicates were used to gauge the measurement error associated with profiling gene expression from 10 'average' cells.

Our analysis focused on the 4,557 transcripts that we clearly identified in all 32 microarrays (16 samplings plus 16 controls, $P < 0.1$). First, we identified the subset of transcripts whose sampling CV was significantly ($P < 0.05$) higher than the corresponding control CV in amplification replicates (Online Methods). We reasoned that the independent samplings of such transcripts would provide a good estimate for normal biological variation with only a minor contribution from measurement noise. We eliminated many transcripts from the subset because their independent 10-cell sampling measurements were highly reproducible. For example, 1,332 genes had a sampling CV <20%, meaning that the corresponding control CV would have needed to be less than ~10% to be included in the analysis. We presumed that the majority of these transcripts were homogeneously expressed or show heterogeneities too small or infrequent to be detected experimentally.

Next, we clustered the independent measurements of the 1,003 genes in the subset, using Euclidean distance as a metric to sort transcripts roughly by sampling CV (**Fig. 3a**). We observed a

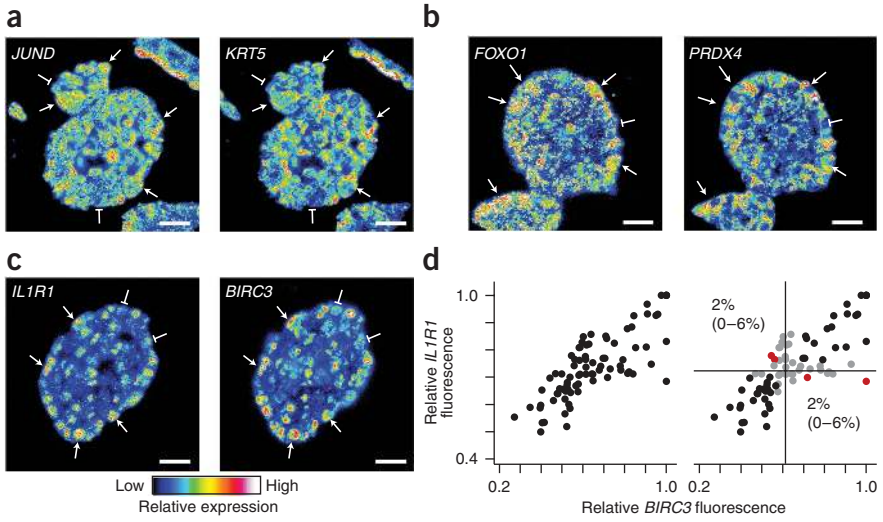

Figure 4 | Stochastic profiling identifies clusters of heterogeneously coexpressed transcripts. (**a**–**c**) Two-color RNA FISH images collected at day 10 of MCF10A morphogenesis for *JUND* and *KRT5* in the protein-synthesis cluster (**a**), *FOXO1* and *PRDX4* in the stress-response cluster (**b**) and *IL1R1* and *BIRC3* in the NF-κB cluster (**c**). Images are pseudocolored to highlight quantitative differences in fluorescence intensity, and single cells showing strong coexpression are highlighted with arrows (high expression) or flat markers (low expression). Scale bars, 20 μm. (**d**) *BIRC3*–*IL1R1* images were segmented to quantify average fluorescence intensities in single cells as described in Online Methods. Data are shown from cells in four independent acini after normalization to the maximum observed cellular fluorescence signal in each image. Gates were defined as the 25th percentile centered on the median fluorescence intensity (black lines) for each gene. Observations that were in the range of the gates were scored as neither positive nor negative (gray). Single positive cells (red) are shown as the percentage of the overall cell population with 90% confidence intervals in parentheses.

plateau of low and consistent sampling CVs, followed by an abrupt increase at which sampling fluctuations seemed to become more irregular and less random. We defined the transcripts in the early plateau as the reference-gene set (**Fig. 3a**) and found that the median sampling CV in this set was 19% with an interquartile range of 14–26% (**Supplementary Fig. 7a**). We fed these empirically derived parameters into our earlier model and found that stochastic profiling should be effective across the entire interquartile range of CVs (**Supplementary Fig. 7b**). Last, we compared sampling fluctuations of individual transcripts to a log-normal reference distribution with $CV_a = 0.19$ at a false discovery rate of 0.05 (**Supplementary Fig. 7c**). Overall, stochastic profiling identified 547 genes whose expression we predicted would be strongly heterogeneous (12% of all transcripts consistently detected).

Discovery of heterogeneous single-cell programs

We standardized and reclustered the sampling data for the candidate heterogeneities to organize genes by their pattern of sampling fluctuations (**Fig. 3b**). The analysis identified multiple clusters that had strong links to recognized biological processes. The first cluster contained many genes involved in protein synthesis, including ribosomal subunits (*RPS6*, *RPL38* and others), initiation-elongation factors (*EIF3M* and *EEF2*) and chaperones (*SEC61G* and *TBCA*). This cluster also contained the basal-progenitor markers, *KRT5* (ref. 22) and an *ALDH* isoform[23], and the *JUND* transcription factor. The second cluster was comprised of several transcripts connected with oxidative-stress responses and proliferative suppression, such as *PRDX4*, *FAM120A*[24], *SERP1* (ref. 25) and *FOXO1* (ref. 26). The third cluster was the smallest but contained a large proportion of genes known to be initiators (*ILIR1*), effectors (*NFKBIA*) or markers (*BIRC3* and *SOD2*) of NF-κB signaling[27]. We also observed heterogenous NF-κB signaling post-translationally by localization of the p65 subunit of NF-κB and expression of IκBα, an upstream inhibitor of NF-κB (**Supplementary Fig. 8**). Taken together, the correlated sampling fluctuations and shared biological function within clusters suggested these were molecular programs that were induced heterogeneously in single cells.

We next validated the stochastic-profiling predictions by an independent method. We developed an RNA fluorescence *in situ* hybridization (FISH) procedure for dual tracking of gene-expression variation in individual cells (Online Methods). We optimized our two-color RNA FISH protocol for specificity (**Supplementary Figs. 9** and **10**) and for reliably detecting single-cell co-regulatory patterns between selected transcripts (**Fig. 4a–c**). Using RNA FISH, we observed pronounced cell-to-cell expression heterogeneities for nearly all transcripts identified by stochastic profiling that we examined (**Fig. 4a–c**, **Supplementary Fig. 11** and **Supplementary Note 1**). Conversely, we observed more-uniform expression for two genes, *GAPDH* and *HINT1*, whose stochastic-sampling fluctuations were not different than the reference distribution (**Supplementary Fig. 12**). Thus, stochastic profiling can separate acute single-cell heterogeneities from transcripts with normal expression variability.

For gene pairs in the same cluster, we found highly concordant patterns of strong and weak expression among individual cells (**Fig. 4a–c**, **Supplementary Fig. 11** and **Supplementary Note 2**). Analysis of cell-to-cell fluorescence intensities revealed that matrix-attached cells were almost exclusively 'double negative' (weakly expressing both genes) or 'double positive' (strongly expressing both genes) (**Fig. 4d**). Cells that strongly expressed one gene but not the other ('single positive') were too rare to constitute a meaningful subpopulation and were likely filtered out by stochastic profiling (**Fig. 4d** and **Supplementary Fig. 1**). Together, this indicates that clusters of genes with similar stochastic-sampling fluctuations were heterogeneously coexpressed with high probability.

As a final validation, we checked whether genes in separate stochastic-profiling clusters were distinguishable on the single-cell level by RNA FISH. The observed concordance between clusters ranged from no discernable correlation (**Fig. 5a–c**) to pairs with stronger covariation (**Fig. 5d–i**). Nevertheless, for each gene pairing, we repeatedly identified single-positive cells at frequencies that should be detected by stochastic profiling (>9–10%, **Figs. 1i** and **5b**,**e**,**h**). Inclusion of these single-positive cells during stochastic sampling would be sufficient to perturb any correlated fluctuations, providing an explanation for the distinct clusters

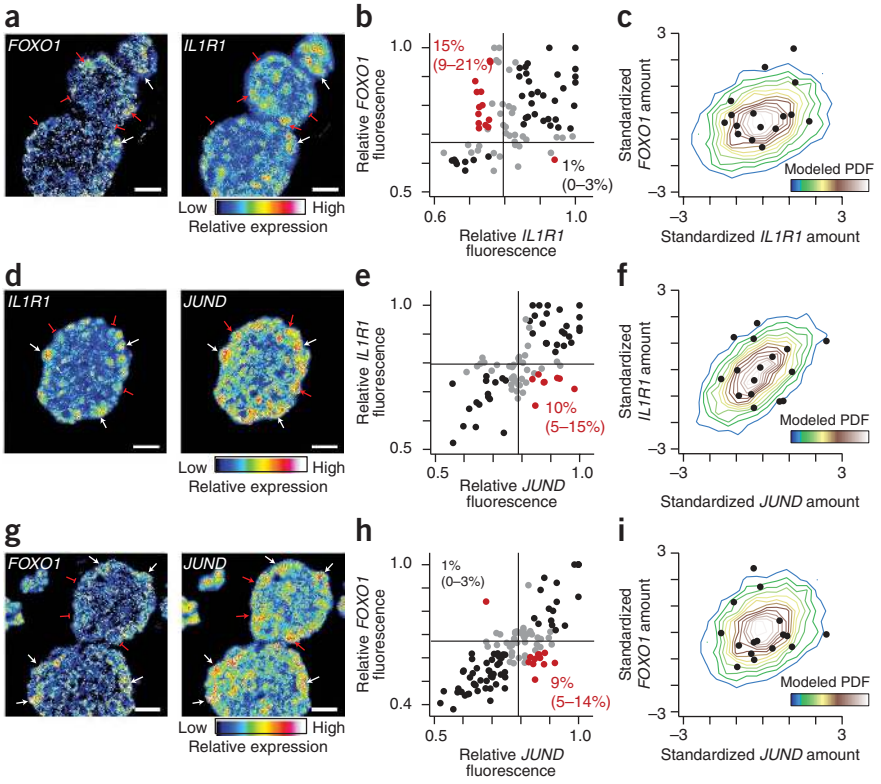

Figure 5 | Stochastic profiling distinguishes heterogeneous expression patterns that are not exclusively coexpressed. (**a**–**i**) Two-color RNA FISH images (**a**,**d**,**g**) were collected at day 10 of MCF10A morphogenesis and compared to the stochastic-profiling data for *FOXO1* and *IL1R1* (**a**–**c**), *IL1R1* and *JUND* (**d**–**f**) and *FOXO1* and *JUND* (**g**–**i**). In two-color RNA FISH images, single-positive cells are highlighted with red arrows (high expression) or flat markers (low expression). Scale bars, 20 μm. Fluorescence intensities (**b**,**e**,**h**) are shown from cells in four independent acini after normalization to the maximum observed cellular fluorescence signal in each image. Gates were defined as the 25th percentile centered on the median fluorescence intensity (black lines) for each gene. Observations that were within the range of the gates were scored as neither positive nor negative (gray). The percentages of single-positive cells (red) in the overall cell population are shown with 90% confidence intervals in parentheses. Predicted patterns of stochastic-sampling fluctuations based on single-cell RNA FISH data (**c**,**f**,**i**). RNA FISH distributions shown in **b**,**e**,**h** were resampled as 10-cell averages and standardized, and the resulting probability density function (PDF) of the indicated gene pairs was compared to the standardized sampling fluctuations of the gene pairs from stochastic profiling (black circles) shown in **Figure 3b**.

shown in **Figure 3b**. Indeed, using the RNA FISH measurements as the basis for simulated stochastic samplings, we estimated probability distributions that largely captured the stochastic-profiling measurements (**Figs. 3b** and **5c**,**f**,**i**).

DISCUSSION

Transcriptional heterogeneities can emerge from purely stochastic cell-fate decisions[1,2,28], but they can also be instructed by differences in the microenvironment[29]. Stochastic profiling does not make a distinction between these heterogeneities but provides a means for identifying them so that the underlying mechanisms can be studied thereafter. The biggest advantage of stochastic profiling is its improved accuracy and reproducibility, which became possible when we measured 10 cells instead of one. Although measurements are not explicitly single-cell, the entire procedure requires only a few hundred cells, meaning that stochastic profiling should be amenable to most *ex vivo* tissue specimens.

By applying stochastic profiling to 3D cultures, we identified many genes not previously suspected to be heterogeneously regulated during morphogenesis. MCF10A cells have a basal-progenitor expression profile[30], suggesting that some heterogeneities could be due to partial differentiation of single cells in three dimensions. The existence of a heterogeneous stress-response program is particularly intriguing because it raises the possibility that individual cells might occupy stressful niches caused by local cell-cell interactions and basement-membrane composition.

Another question is whether the single-cell programs identified by stochastic profiling are coordinated during morphogenesis. For the gene clusters imaged simultaneously by RNA FISH, we found that the single-positive populations were not equally populated. For example, high *JUND* expression could be found in cells with low *IL1R1* or *FOXO1* expression, but cells with the opposite pattern were extremely rare (**Fig. 5e**,**h**). Future work will focus in greater depth on these dependencies and their possible role during morphogenesis.

The extent to which heterogeneously activated pathways *in vivo* might obscure phenotypes or create patterns in tissues is only beginning to be studied[1]. The bottleneck is not in studying the role of heterogeneities but in identifying them in the first place. Stochastic profiling provides a valuable tool for analyzing the coordination of such pathways quantitatively and systematically.

METHODS

Methods and any associated references are available in the online version of the paper at http://www.nature.com/naturemethods/.

Note: Supplementary information is available on the Nature Methods website.

ACKNOWLEDGMENTS

We thank T. McDaniel (Illumina) for generously providing the microarrays used in this study, G. Cox (Molecular Probes) for advice during development of the RNA FISH protocol and C. Reinhardt for critically reading the manuscript. This work was supported by the US National Institutes of Health (5-R01-CA105134-07 to J.S.B.), the US National Institutes of Health Director's New Innovator Award Program (1-DP2-OD006464-01 to K.A.J.), the Mary Kay Ash Charitable Foundation (to K.A.J.) and the Pew Scholars Program in the Biomedical Sciences (to K.A.J.).

AUTHOR CONTRIBUTIONS

K.A.J. conceived of the study, performed the computational simulations, designed and optimized the experimental protocols, performed the stochastic profiling experiments, analyzed the data and wrote the initial draft of the manuscript. C.C.W. validated the RNA FISH riboprobes, performed the RNA

FISH experiments and edited the manuscript. K.J.H. cloned and prepared the RNA FISH riboprobes, segmented the images for quantitation and edited the manuscript. K.C. optimized the microarray hybridization protocols and performed the microarray hybridization experiments. J.S.B. supervised the overall research progress and contributed to the initial draft of the manuscript.

COMPETING FINANCIAL INTERESTS

The authors declare no competing financial interests.

Published online at http://www.nature.com/naturemethods/.
Reprints and permissions information is available online at http://npg.nature.com/reprintsandpermissions/.

1. Wernet, M.F. *et al.* Stochastic spineless expression creates the retinal mosaic for colour vision. *Nature* **440**, 174–180 (2006).
2. Chang, H.H., Hemberg, M., Barahona, M., Ingber, D.E. & Huang, S. Transcriptome-wide noise controls lineage choice in mammalian progenitor cells. *Nature* **453**, 544–547 (2008).
3. Irish, J.M., Kotecha, N. & Nolan, G.P. Mapping normal and cancer cell signalling networks: towards single-cell proteomics. *Nat. Rev. Cancer* **6**, 146–155 (2006).
4. Ferrell, J.E. Jr. & Machleder, E.M. The biochemical basis of an all-or-none cell fate switch in *Xenopus* oocytes. *Science* **280**, 895–898 (1998).
5. Altan-Bonnet, G. & Germain, R.N. Modeling T cell antigen discrimination based on feedback control of digital ERK responses. *PLoS Biol.* **3**, e356 (2005).
6. Emmert-Buck, M.R. *et al.* Laser capture microdissection. *Science* **274**, 998–1001 (1996).
7. Tietjen, I. *et al.* Single-cell transcriptional analysis of neuronal progenitors. *Neuron* **38**, 161–175 (2003).
8. Bahar, R. *et al.* Increased cell-to-cell variation in gene expression in ageing mouse heart. *Nature* **441**, 1011–1014 (2006).
9. Fraser, H.B., Hirsh, A.E., Giaever, G., Kumm, J. & Eisen, M.B. Noise minimization in eukaryotic gene expression. *PLoS Biol.* **2**, e137 (2004).
10. Kurimoto, K. *et al.* An improved single-cell cDNA amplification method for efficient high-density oligonucleotide microarray analysis. *Nucleic Acids Res.* **34**, e42 (2006).
11. Debnath, J. & Brugge, J.S. Modelling glandular epithelial cancers in three-dimensional cultures. *Nat. Rev. Cancer* **5**, 675–688 (2005).
12. Golding, I., Paulsson, J., Zawilski, S.M. & Cox, E.C. Real-time kinetics of gene activity in individual bacteria. *Cell* **123**, 1025–1036 (2005).
13. Bengtsson, M., Stahlberg, A., Rorsman, P. & Kubista, M. Gene expression profiling in single cells from the pancreatic islets of Langerhans reveals lognormal distribution of mRNA levels. *Genome Res.* **15**, 1388–1392 (2005).
14. Newman, J.R. *et al.* Single-cell proteomic analysis of *S. cerevisiae* reveals the architecture of biological noise. *Nature* **441**, 840–846 (2006).
15. Brady, G. & Iscove, N.N. Construction of cDNA libraries from single cells. *Methods Enzymol.* **225**, 611–623 (1993).
16. Hartmann, C.H. & Klein, C.A. Gene expression profiling of single cells on large-scale oligonucleotide arrays. *Nucleic Acids Res.* **34**, e143 (2006).
17. Taniguchi, K., Kajiyama, T. & Kambara, H. Quantitative analysis of gene expression in a single cell by qPCR. *Nat. Methods* **6**, 503–506 (2009).
18. Schmelzle, T. *et al.* Functional role and oncogene-regulated expression of the BH3-only factor Bmf in mammary epithelial anoikis and morphogenesis. *Proc. Natl. Acad. Sci. USA* **104**, 3787–3792 (2007).
19. Debnath, J., Walker, S.J. & Brugge, J.S. Akt activation disrupts mammary acinar architecture and enhances proliferation in an mTOR-dependent manner. *J. Cell Biol.* **163**, 315–326 (2003).
20. Pearson, G.W. & Hunter, T. Real-time imaging reveals that noninvasive mammary epithelial acini can contain motile cells. *J. Cell Biol.* **179**, 1555–1567 (2007).
21. Pearson, G.W. & Hunter, T. PI-3 kinase activity is necessary for ERK1/2-induced disruption of mammary epithelial architecture. *Breast Cancer Res.* **11**, R29 (2009).
22. Rakha, E.A., Reis-Filho, J.S. & Ellis, I.O. Basal-like breast cancer: a critical review. *J. Clin. Oncol.* **26**, 2568–2581 (2008).
23. Ginestier, C. *et al.* ALDH1 is a marker of normal and malignant human mammary stem cells and a predictor of poor clinical outcome. *Cell Stem Cell* **1**, 555–567 (2007).
24. Tanaka, M. *et al.* A novel RNA-binding protein, Ossa/C9orf10, regulates activity of Src kinases to protect cells from oxidative stress-induced apoptosis. *Mol. Cell. Biol.* **29**, 402–413 (2009).
25. Yamaguchi, A. *et al.* Stress-associated endoplasmic reticulum protein 1 (SERP1)/Ribosome-associated membrane protein 4 (RAMP4) stabilizes membrane proteins during stress and facilitates subsequent glycosylation. *J. Cell Biol.* **147**, 1195–1204 (1999).
26. Gross, D.N., van den Heuvel, A.P. & Birnbaum, M.J. The role of FoxO in the regulation of metabolism. *Oncogene* **27**, 2320–2336 (2008).
27. Karin, M. & Ben-Neriah, Y. Phosphorylation meets ubiquitination: the control of NF-[kappa]B activity. *Annu. Rev. Immunol.* **18**, 621–663 (2000).
28. Laslo, P. *et al.* Multilineage transcriptional priming and determination of alternate hematopoietic cell fates. *Cell* **126**, 755–766 (2006).
29. Yakoby, N. *et al.* A combinatorial code for pattern formation in *Drosophila* oogenesis. *Dev. Cell* **15**, 725–737 (2008).
30. Neve, R.M. *et al.* A collection of breast cancer cell lines for the study of functionally distinct cancer subtypes. *Cancer Cell* **10**, 515–527 (2006).

ONLINE METHODS

Monte Carlo simulations. Stochastic sampling simulations (**Fig. 1**) were performed in Matlab (Mathworks) with the statistics toolbox. For each simulation, the model assumed a binomial distribution for the cellular dichotomy and log-normal distribution of measured transcripts[13,31]. CV_a and CV_b were varied between 12–38% to approximate biologically plausible values[14] and then rerun with empirically derived values (**Supplementary Fig. 7a**,**b**). The distribution of 48 population-averaged samplings was log-mean centered and compared to a log-normal distribution with an s.d. estimated from 48 reference samplings. The χ^2 goodness of fit between the dichotomous and reference distributions was done using the chi2gof function with 10 bins. The χ^2 test directly evaluates the relative differences between observed and expected values on the sampling histogram and is a robust, conservative test for this application[32]. Bins were pooled if the observed or expected value in a bin was less than five. Each CV_a, CV_b, D and F parameter set was run 50 times to measure the median P values and the associated nonparametric confidence intervals. Stochastic sampling was deemed effective when the median P value for $F \neq 0$ was less than 0.05 and the median P value for $F = 0$ was greater than 0.05. The source code for the simulations is available in **Supplementary Software**.

For the simulation of probability density functions (**Fig. 5c**,**f**,**i**), the single-cell FISH intensities from **Figure 5b**,**e**,**h** were randomly combined as 10-cell averages for each gene pair for 5,000 iterations. These bootstrapped estimates were standardized and then compiled as two-dimensional histograms by using the hist2 function with 20 bins.

Cell lines. The MCF10A-5E clone was isolated by limiting dilution of the parental MCF10A line (American Type Culture Collection) and selected for its homogeneous behavior in 3D culture. MCF10A-5E cells were maintained as described previously for MCF10A cells[33].

Frozen sectioning of 3D cultures. To allow embedding of 3D cultures, a plastic coverslip was cut to size and placed at the base of an 8-well chamber slide (BD Biosciences) before starting. Coverslip-covered chamber slides were then coated with Matrigel (BD Biosciences), and 3D culture of MCF10A-5E cells was performed as described previously[33]. For fresh frozen sections (used for laser capture microdissection), coverslips were washed with PBS and then embedded directly in Neg-50 (Richard-Allan Scientific) on a dry ice–isopentane bath. For fixed frozen sections (used for RNA FISH), coverslips were washed in PBS and fixed in 3.7% paraformaldehyde for 15 min. After three 5 min washes in PBS, samples were cryopreserved in 15% sucrose for 15 min, 30% sucrose for 15 min and then embedded in Neg-50 as described above. Sectioning was performed at −24 °C on a cryostat (Leica). Embedded specimens and cryosections were stored at −80 °C until further use.

Laser capture microdissection. We cut 8 μm sections on plain glass slides and kept them at −24 °C during sectioning and −80 °C during storage. After removing the samples from −80 °C storage, slides were fixed immediately in 75% ethanol for 30 s, followed by distilled water for 30 s. Fixed slides were stained for 30 s with nuclear fast red (Vector Laboratories) containing 1 U ml^{-1} RNAsin Plus (Promega), then washed twice in distilled water for 15 s. Stained slides were dehydrated with an ethanol series (30 s each of 70%, 95% and 100% ethanol) and cleared with xylene for 2 min. After air-drying for 5–10 min, slides were stored in a dessicator and used immediately.

Before microdissection, slides were cleaned with a PrepStrip (Arcturus) to remove loosely adhered material. Microdissection was performed on a Pixcell II instrument (Arcturus) using Capsure HS LCM caps (Arcturus). We used 750 μs laser shots at 50–65 mW power to achieve single-cell resolution (**Supplementary Fig. 6**). For this study, matrix-attached cells were sampled at 3–4 random positions across ~3 acini to focus on matrix-dependent (rather than acinus-dependent) heterogeneities. After microdissection, LCM caps were cleaned with an adhesive note to remove biological material next to the dissected cells.

Small-sample quantitative mRNA amplification. Samples were eluted from the microdissection caps by adding 4 μl digestion buffer (1.25× MMLV reverse transcriptase buffer (Invitrogen), 100 μM dNTPs (Roche), 0.08 OD ml^{-1} oligo$(dT)_{24}$ and 250 μg ml^{-1} proteinase K (Sigma)) and incubating at 42 °C for 1 h. Digested samples were centrifuged into PCR tubes and quenched with 1 μl of digestion stop buffer (1.5 U ml^{-1} Prime RNAse inhibitor (Eppendorf), 1.5 U ml^{-1} RNAguard (Amersham) and 5 mM freshly prepared PMSF). The quenched samples were then processed by using poly(A) PCR[15] that we modified to allow quantitative amplification of high- and low-abundance transcripts.

We transferred 4.5 μl of the quenched samples into thin-walled 0.2-ml PCR tubes and added 0.5 μl of Superscript III (Invitrogen). The first-strand synthesis reaction was incubated at 50 °C for 15 min and then heat-inactivated at 70 °C for 15 min. The samples were placed on ice and centrifuged for 2 min at 18,000*g* on a benchtop centrifuge at 4 °C. Next, 1 μl of RNAse H solution (2.5 U ml^{-1} RNAse H (USB Corporation) and 12.5 mM $MgCl_2$) was added, and the reaction was incubated at 37 °C for 15 min. After RNAse H treatment, the reaction was poly(A)-tailed with 3.5 μl of 2.6× tailing solution (80 U terminal transferase (Roche), 2.6× terminal transferase buffer (Invitrogen) and 1.9 mM dATP) for 15 min at 37 °C and then heat-inactivated at 65 °C for 10 min. The samples were placed on ice and spun for 2 min at 18,000*g* on a benchtop centrifuge at 4 °C. To each sample, 90 μl of ThermoPol PCR buffer was added to a final concentration of 1× ThermoPol buffer (New England Biolabs), 2.5 mM $MgSO_4$, 1 mM dNTPs (Roche), 100 μg ml^{-1} BSA (Roche), 10 U AmpliTaq (Applied Biosystems) and 5 μg AL1 primer[15]. Each reaction was split into three thin-walled 0.2-ml PCR tubes and amplified according to the following thermal cycling scheme: four cycles of 1 min at 94 °C (denaturation), 2 min at 32 °C (annealing) and 6 min plus 10 s per cycle at 72 °C (extension); 21 cycles of 1 min at 94 °C (denaturation), 2 min at 42 °C (annealing) and 6 min 40 s plus 10 s per cycle at 72 °C (extension). The tubes were cooled, placed on ice and the reactions from three tubes for each sample were pooled and amplified according to the following thermal cycling scheme: five cycles of 1 min at 94 °C (denaturation), 2 min at 42 °C (annealing) and 6 min at 72 °C (extension). Additional thermal cycling led to overamplification and loss of quantitative accuracy (K.A.J. and J.S.B., unpublished observations). Samples were stored at −20 °C until use.

Real-time qPCR. Real-time qPCR of amplified material from stochastic sampling was measured as described previously[34], except

doi:10.1038/nmeth.1442

that tenfold less of each amplified sample was used as the starting cDNA template. Primer sequences and concentrations are shown in **Supplementary Table 1**.

Small-sample reamplification and microarray hybridization. Amplified small-sample poly(A) PCR cDNA samples were reamplified and aminoallyl labeled in a 100 µl reaction containing 1× High-Fidelity buffer (Roche), 3.5 mM $MgCl_2$, 200 µM dATP, dCTP, and dGTP, 40 µM dTTP (Roche), 160 µM aminoallyl-dUTP (Ambion), 100 µg ml^{-1} BSA (Roche), 5 µg AL1 primer and 1 µl amplified cDNA. Each reaction was amplified according to the following thermal cycling scheme: 1 min at 94 °C (denaturation), 2 min at 42 °C (annealing) and 3 min at 72 °C (extension). In pilot experiments, 20 µl of this reaction for each stochastic sampling was monitored in the presence of 0.25× SYBR Green on a LightCycler II real-time PCR instrument (Roche). The number of amplification cycles (~20) was selected to ensure that all samples remained in the exponential phase during amplification[35]. Samples were purified on a PureLink column (Invitrogen), ethanol-precipitated and labeled with Alexa Fluor 555 amine-reactive dye (Invitrogen) according to the manufacturer's recommendation. Labeling efficiency was ~2 dye molecules per 100 bases.

For microarray hybridization, 1 µg Alexa Fluor 555–labeled cDNA (total volume, 5 µl) was mixed with 10 µl GEX hybridization buffer (Illumina). Samples were denatured at 94 °C for 4 min and then added directly to HumanRef-8 Expression BeadChips (Illumina) prewarmed to 58 °C. Slides were incubated at 58 °C for 20 h and washed according to the manufacturer's recommendations. After drying, slides were scanned on a BeadArray reader (Illumina) with a scan setting of "Direct hybridization 1." Samples were normalized to their mean overall fluorescence intensity relative to the overall dataset and then to the median fluorescence intensity of all transcripts detected ($P < 0.1$) on each sample for subsequent analysis.

Riboprobe synthesis. A 175–225 bp fragment of each gene was cloned by PCR into pcDNA3 (Invitrogen) from an MCF10A cDNA library generated by first-strand synthesis with Superscript III (Invitrogen) and an oligo$(dT)_{24}$ primer. Plasmids were linearized with the appropriate restriction enzymes and purified by phenol-chloroform extraction and ethanol precipitation. Riboprobes were synthesized from the linearized template by using the MAXIscript Sp6/T7 kit (Ambion) as recommended, except that *in vitro* transcriptions were incubated for 2 h and Sp6 *in vitro* transcriptions were performed at 40 °C to increase yield. Digoxigenin (DIG)- and dinitrophenyl (DNP)-labeled riboprobes were synthesized with 35 mol% DIG–UTP (Roche) or DNP-UTP (Perkin Elmer) and 65 mol% unlabeled UTP. After DNAse digestion, riboprobes were ethanol-precipitated, resuspended in RNAse-free water to 0.2 µg ml^{-1} and stored at −80 °C. The specificity of riboprobes was evaluated by comparing the antisense RNA FISH signal intensity to the corresponding sense riboprobe (**Supplementary Figs. 9** and **10** and **Supplementary Note 3**).

Multicolor RNA fluorescence *in situ* hybridization (FISH). We cut 5 µm frozen sections of day 10 3D structures on Superfrost Plus slides (Fisher), air-dried them and stored them at −80 °C. Slides were thawed at room temperature (23 °C) until completely dry, treated with 0.2 N HCl for 10 min and washed in PBS for 5 min. Slides were then fixed in 3.7% paraformaldehyde for 15 min, washed twice for 10 min in PBS and once in freshly prepared 0.1 M triethanolamine (pH 8.0) for 10 min. Samples were next acetylated with 0.25% acetic anhydride in freshly prepared 0.1 M triethanolamine (pH 8.0) for 5 min and washed in 2× SSC for 10 min. Slides were dehydrated with an ethanol series (2 min each of 70%, 95% and 100% ethanol), and sections were covered with hybridization solution (1 mg ml^{-1} yeast tRNA, 10% dextran sulfate in 2× SSC, 50% formamide) containing 50–500 ng ml^{-1} of each riboprobe. Sections were covered with Parafilm, sealed with rubber cement and incubated at 42 °C in a humidified chamber for 14–16 h.

After hybridization, slides were soaked in 2× SSC at 37 °C for 5 min, the Parafilm was removed and slides were washed in 2× SSC, 50% formamide for 30 min at 55 °C, followed by 0.1× SSC for 30 min at 55 °C. Slides were equilibrated in PBS for 10 min and then blocked for 1 h at room temperature with 1× Western Blocking reagent (Roche) in PBS with 0.3% Tween-20. After blocking, slides were incubated 1 h at room temperature with 1× Western Blocking reagent in PBS with 0.3% Tween-20 containing anti-digoxin (1:500; Jackson ImmunoResearch) and anti-DNP (1:1,000; Invitrogen). Slides were washed three times for 5 min in PBS and incubated for 1 h at room temperature with 1× Western Blocking reagent in PBS with 0.3% Tween-20 containing Alexa Fluor 488–conjugated goat anti-rabbit (1:200; Invitrogen) and Alexa Fluor 555–conjugated goat anti-mouse (1:200; Invitrogen). Slides were washed three times for 5 min in PBS and cell membranes were labeled with 20 µg ml^{-1} Alexa Fluor 350–conjugated wheat-germ agglutinin for 5 min at room temperature. After two 5 min washes in PBS, autofluorescence was quenched with 10 mM $CuSO_4$ in 50 mM NH_4Ac (pH 5.0) for 10 min[36]. Slides were washed with PBS for 5 min and mounted with 0.5% n-propyl gallate in PBS with 90% glycerol[37].

Immunofluorescence. We cut 5 µm sections of day 10 3D structures on Superfrost Plus slides (Fisher), air-dried and stored at −80 °C until further use. Slides were thawed at room temperature until completely dry, hydrated three times for 5 min in PBS and then blocked for 1 h at room temperature with 1× Western Blocking reagent in PBS with 0.3% Tween-20. After blocking, slides were incubated overnight at room temperature with 1× Western Blocking reagent in PBS with 0.3% Tween-20 containing anti-p65 (A) (1:100; Santa Cruz) or anti-IκBα (C-21) (1:500; Santa Cruz). Slides were washed three times for 5 min in PBS and incubated for 1 h at room temperature with 1× Western Blocking reagent in PBS with 0.3% Tween-20 containing Alexa Fluor 555–conjugated goat anti-rabbit (1:200; Invitrogen). Slides were washed three times for 5 min in PBS and counterstained with 0.5 µg ml^{-1} DAPI (Sigma) for 5 min at room temperature. After two 5 min washes in PBS, autofluorescence was quenched with 10 mM $CuSO_4$ in 50 mM NH_4Ac (pH 5.0) for 10 min[36]. Slides were washed with PBS for 5 min and mounted with 0.5% n-propyl gallate in PBS with 90% glycerol[37].

Microscopy. Frozen sections and coverslips were imaged with a 40× 1.3 numerical aperture (NA) oil objective on a BX51 upright fluorescence microscope (Olympus) with the following filter sets: ET-DAPI (excitation, 325–375 nm; dichroic, 400 nm; and emission, 435–485 nm), ET-FITC (excitation, 450–490 nm;

dichroic, 495 nm; and emission, 500–550 nm), ET-CY3 (excitation, 520–570 nm; dichroic, 565 nm; and emission, 570–640 nm) and ET-CY5 (excitation, 590–650 nm; dichroic, 660 nm; and emission, 665–735 nm). Images were captured with an Orca R2 CCD camera (Hamamatsu) at 2 × 2 binning and exposure times that filled 90% of the camera bit depth, with the exception of the RNA FISH sense controls (**Supplementary Figs. 9** and **10**) where the exposure time was matched to the antisense image. Displayed images were rainbow-pseudocolored with a linear lookup table that covered the full range of the data for each fluorescence channel.

Image segmentation and quantification. Single cells from RNA FISH images were segmented by hand based on wheat-germ agglutinin staining (DAPI channel), and traced image segments were then applied to the DIG- and DNP-labeled riboprobe stainings (FITC and Cy3 channels). Median fluorescence intensities per cell for each riboprobe were calculated, and individual images were normalized to the maximum observed intensity in each channel for comparison across multiple images.

Statistical analysis. Statistical analyses of real-time qPCR measurements were performed on the cycle thresholds of the measured genes. This is equivalent to a $\log_2$ transformation, which allows log-normal distributions to be treated as normal distributions[13,31]. Estimation of the coefficient of variation for amplification replicates (**Fig. 2i**) was done in Igor Pro (WaveMetrics) by nonlinear least-squares curve fitting of the mean-centered cycle thresholds to a normal distribution with a mean of zero. Confidence intervals on CVs were calculated with McKay's transformation[38], and non-overlapping 90% confidence intervals were considered significantly different ($P < 0.05$)[39]. χ^2 goodness-of-fit tests for sampling fluctuations were performed in MATLAB with the chi2gof function, a mean of zero and an s.d. equal to the reference distribution (false discovery rate = 0.05). Nonparametric confidence intervals for the RNA FISH subpopulations were based on a binomial distribution.

31. Warren, L., Bryder, D., Weissman, I.L. & Quake, S.R. Transcription factor profiling in individual hematopoietic progenitors by digital RT-PCR. *Proc. Natl. Acad. Sci. USA* **103**, 17807–17812 (2006).
32. Sheskin, D.J. *Handbook of Parametric and Nonparametric Statistical Procedures* 4th edn. (Chapman & Hall, New York, 2007).
33. Debnath, J., Muthuswamy, S.K. & Brugge, J.S. Morphogenesis and oncogenesis of MCF-10A mammary epithelial acini grown in three-dimensional basement membrane cultures. *Methods* **30**, 256–268 (2003).
34. Miller-Jensen, K., Janes, K.A., Brugge, J.S. & Lauffenburger, D.A. Common effector processing mediates cell-specific responses to stimuli. *Nature* **448**, 604–608 (2007).
35. Nagy, Z.B. *et al.* Real-time polymerase chain reaction-based exponential sample amplification for microarray gene expression profiling. *Anal. Biochem.* **337**, 76–83 (2005).
36. Schnell, S.A., Staines, W.A. & Wessendorf, M.W. Reduction of lipofuscin-like autofluorescence in fluorescently labeled tissue. *J. Histochem. Cytochem.* **47**, 719–730 (1999).
37. Giloh, H. & Sedat, J.W. Fluorescence microscopy: reduced photobleaching of rhodamine and fluorescein protein conjugates by n-propyl gallate. *Science* **217**, 1252–1255 (1982).
38. McKay, A.T. Distribution of the coefficient of variation and the extended 't' distribution. *J. R. Stat. Soc. A* **95**, 695–698 (1932).
39. Julious, S.A. Using confidence intervals around individual means to assess statistical significance between two means. *Pharm. Stat.* **3**, 217–222 (2004).

doi:10.1038/nmeth.1442